

Microscopic tensile deformation mechanisms in bulk polyamide 6

C. Millot^{1,2}, L.-A. Fillot¹, O. Lame², R. Séguéla², P. Sotta¹

¹Laboratoire Polymères et Matériaux Avancés, CNRS, Solvay, Saint-Fons, France.

²Laboratoire Mateis, INSA Lyon, CNRS, Villeurbanne, France.

Summary: Microscopic deformation mechanisms in bulk PA6 under uniaxial stretching are studied in both the elastic and plastic regimes up to fibrillation, by in-situ combined Wide and Small Angle X ray Scattering. Different scenarios are described depending on the type of crystalline phase (α , γ , β) and on the test temperature.

Introduction

To improve thermo-mechanical performances of semi-crystalline thermoplastic polymers used for structural applications, it is of prime importance to understand the mechanisms of deformation in relation to the microstructure, which implies multi-scale investigations. Polyolefins, mostly polyethylene or polypropylene, have been widely studied in this context [1,2]. Few models have been developed in order to link the different scales [3]. Polyamides are more complex materials, due to H-bonds and a generally rich polymorphism [4,5]. For polyamide 6 (PA6), most studies have concerned fibers or thin films [6-8].

Here we investigate the microscopic deformation mechanisms which occur in bulk PA6 under uniaxial stretching below and above yield, with a multi-scale experimental approach, at the scale of the crystalline unit cell as well as at the scale of the lamellar stackings. By various thermal treatments, we have prepared PA6 samples in which the crystalline phase is either predominantly α or β . We propose a quantitative analysis of deformation mechanisms. We show that different scenarios occur during tensile tests up to fibrillation, depending on the crystalline phase and temperature.

Samples and methods

PA6 samples ($M_n = 31 \text{ kg}\cdot\text{mol}^{-1}$, polydispersity index 1.86) in which the crystalline phase is predominantly α or β have been obtained by various thermal treatments, based on few reported studies [9-14] (see Table 1). The INJ (injection moulded) sample contains predominantly β phase, with some small amount of γ . It shows a large number of small spherulites. I213 was maintained for 10 min in the melt at 270°C (in order to erase memory effects) then quenched rapidly down to 213°C (small undercooling) and isothermally crystallized at this temperature. I213 contains predominantly α phase. It shows relatively large, well-formed spherulites. Crystalline phases were characterized by Wide Angle X ray Scattering (WAXS), long periods by Small Angle X ray Scattering (SAXS), crystallinity ratios by DSC. In-situ tensile tests with combined WAXS and SAXS were performed on beamline BM2, ESRF, Grenoble, using a home-built, variable temperature stretching device. Scattered intensity patterns collected on a 2D detector are analyzed as a function of the azimuthal angle ψ with respect to the tensile direction (TD).

Results

Stress-strain curves obtained in tensile tests performed above T_g ($T = 120^\circ\text{C}$, a) and below T_g ($T = -10^\circ\text{C}$, b) are shown in Figure 1, together with examples of SAXS patterns recorded in-situ. In SAXS, scattering by a lamellar stack gives a correlation peak in the direction perpendicular to the lamella surfaces. Peak intensity in an azimuthal direction ψ from TD comes from lamellar planes perpendicular to this direction and thus gives the relative number of lamellae with normal oriented at angle ψ . The scattering vector q_{max} at peak maximum gives the long period of the lamellar stacking $L_p = 2\pi/q_{max}$.

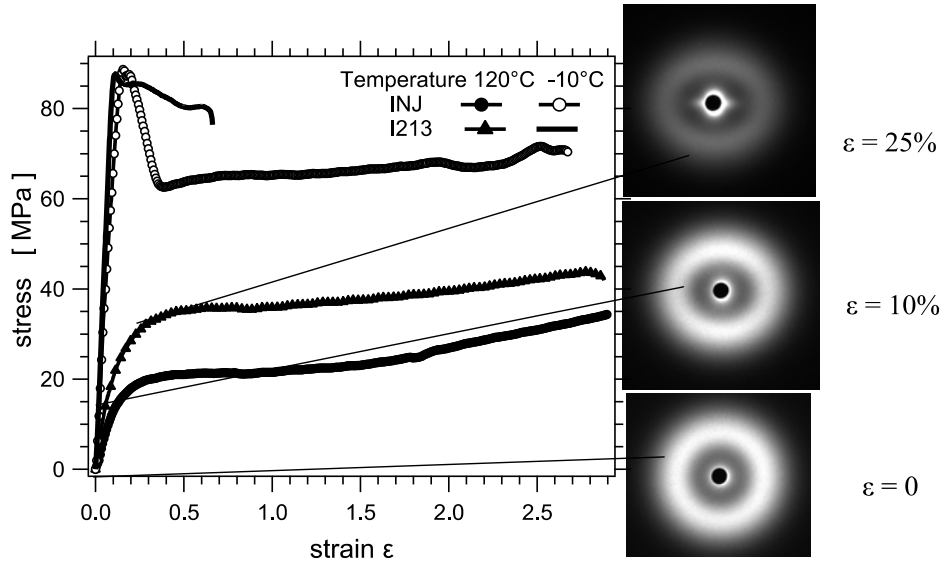


Figure 1: Stress-strain curves at $\dot{\epsilon} = 3 \times 10^{-3} \text{ s}^{-1}$ at $T = -10^\circ\text{C}$ and 120°C , for INJ and I213 samples, with SAXS patterns measured at different strain values.

The relative variation $\Delta L_p/L_p$ is plotted in Figure 2(a) as a function of ψ , for different values of the strain ϵ . L_p increases (resp. decreases) along (resp. perpendicular to) TD. The local strain along TD $\Delta L_p/L_p(\psi = 0)$ is plotted vs the strain ϵ in Figure 2(b).

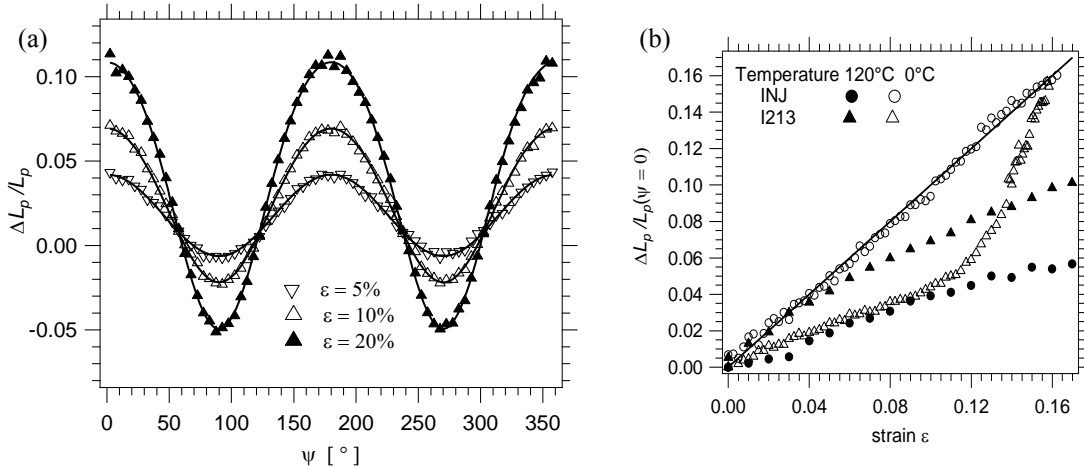


Figure 2: (a): relative variation $\Delta L_p/L_p$ in sample I213 as a function of the angle ψ with respect to TD, for different strain values at $T = 120^\circ\text{C}$. (b): $\Delta L_p/L_p(\psi = 0)$ (along TD) as a function of the strain ϵ .

The variation of intensity as a function of ψ is shown in Figure 3(a). The intensity is reinforced for $\psi = 0 \pmod{\pi}$, indicating that lamellae tend to orient with their normals along TD, i.e with their planes perpendicular to TD.

In a homogeneous material uniaxially stretched along z , the only non-zero element of the stress tensor $\bar{\sigma}$ is σ_{zz} . A material vector \vec{dr} at angle ψ from TD will be distorted into \vec{dr}' such that $\|\vec{dr}'\| \cong \|\vec{dr}\| [1 + (1/3)(1 - 2\nu)(\sigma_{zz}/E) + (2/3)(1 + \nu)(\sigma_{zz}/E)P_2(\cos \psi)]$ (Figure 2(b)) where E and ν are Young's and Poisson's moduli, respectively, and $P_2(\cos \psi) = (3\cos^2 \psi - 1)/2$ is the 2nd order Legendre polynomial [15]. Thus, identifying the relative variation (or local strain) $\Delta L_p/L_p$ to this relative length variation gives

$$\frac{\Delta L_p}{L_p} = \frac{\epsilon}{3} [(1 - 2\nu) + 2(1 + \nu)P_2(\cos \psi)] \quad (1)$$

where $\epsilon = \sigma_{zz}/E$ is the macroscopic strain. Thus, comparing experimental data to Eq. (1) shall indicate how much the local strain at the scale of crystalline lamellae deviates from the (uniform) macroscopic strain.

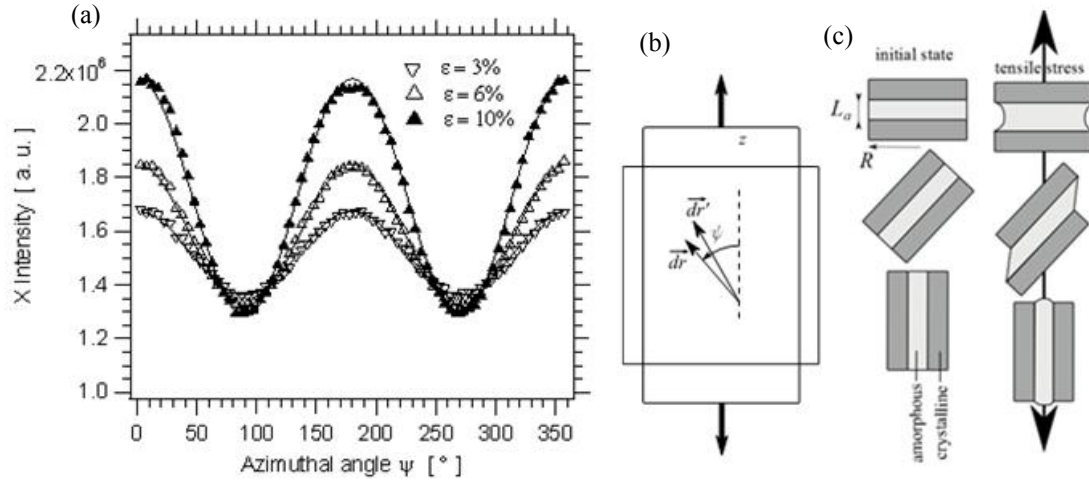


Figure 3: (a): intensity as a function of ψ for different strain values : a) at $T = -10^\circ\text{C}$ and b) $T = 120^\circ\text{C}$ for I213 and INJ samples. (b): local deformation of a vector at angle ψ from tensile direction. (c) : non homogeneous tensile deformation.

The same analysis may be adopted to describe the distribution of lamella orientations, by assuming that the normal \vec{n} to a lamella deforms affinely under uniaxial stretching, which gives a relative number of lamella within the interval $[\psi, \psi + d\psi]$

$$n_\varepsilon(\psi)d\psi \approx \frac{(1 + \varepsilon)^3 \sin \psi}{(\cos^2 \psi + (1 + \varepsilon)^3 \cos^2 \psi)^{3/2}} d\psi \quad (2)$$

Comparing experimental data (Figure 3) to Eq. (2) indeed indicates that the distribution of lamella normals tend to be deformed affinely in the INJ sample and in the I213 sample drawn at 0°C . Equivalently, lamellae tend to orient perpendicular to the tensile direction.

It is observed (Figure 2b) that the local strain (at $\psi = 0$) is smaller than the macroscopic strain, specifically above T_g . Indeed, restricted lateral constriction increases the effective Young's modulus of horizontal stacks. The resulting decreased strain must be compensated by amplified shear deformation of inclined stacks [16] (which however cannot be detected by SAXS) (Figure 3c).

For the INJ sample (predominant β phase), morphology changes are illustrated on WAXS patterns shown in Figure 4a. Here the ring intensity comes from lattice planes which are perpendicular to lamellar planes. Horizontal scattering ($\psi = 90^\circ$) thus comes from horizontal lamellae (perpendicular to TD). The tendency of the lamellae to orient perpendicular to the tensile direction in the elastic domain (step a2 in Figure 4a) amplifies until a highly oriented fibrillar morphology is obtained (step a3 in Figure 4a). Then, it is observed also that the β phase initially present transforms into α phase after some delay (step a4 in figure 4a).

The observed behavior is more complex in the I213 sample drawn at 120°C . In this case, WAXS patterns (Figure 4b) show two well-resolved rings, characteristic of the α phase, corresponding to the three families of lattice planes containing chain axis. The intensity in the inner ring, corresponding to (200) planes, is first reinforced in the tensile direction (step b2 in Figure 4b), which means that corresponding planes orient perpendicular to the tensile direction. In this configuration, chain axis must be perpendicular to the tensile direction. Then, at higher strain, beyond the yield point, chains reorient along the tensile direction so that lamellae are ultimately perpendicular to the tensile direction (step b3 in Figure 4b).

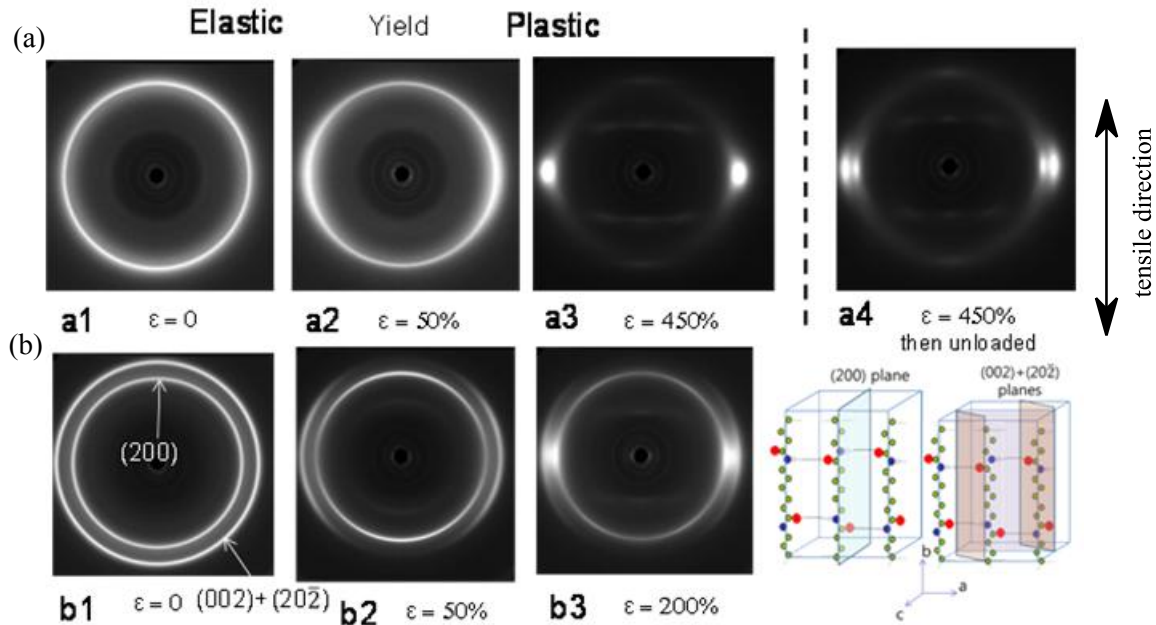


Figure 4. WAXS patterns at different strain values at $T = 120^{\circ}\text{C}$: (a): INJ sample; (b): I213 sample

Conclusion

In samples with predominantly β phase, the deformation is qualitatively described by affine deformation of the lamella normals. Lamellae tend to orient perpendicular to TD. The tensile strain in lamellar stacks perpendicular to TD is lower than the macroscopic tensile strain, which must be compensated by increased shear in inclined stacks. In samples with predominantly α phase, morphology changes are more complex. In a first step, some lattice planes orient perpendicular to TD, which implies that chains are perpendicular to TD. Beyond yield, lamellae reorient with their normal perpendicular to TD, thus chains themselves become parallel to TD, leading to a highly oriented fibrillar morphology as well.

Acknowledgements

The authors are indebted to the European Synchrotron Radiation Facility (Grenoble, France) for time allocation on the BM02 beamline.

References

- [1] Humbert S.; Lame O.; Chenal J. M., et al. *J Polym Sci, Polym Phys* **2010**, *48*, 1535.
- [2] Humbert S.; Lame O.; Vigier G., *Polymer* **2009**, *50*, 3755.
- [3] Nikolov S.; Doghri I.; Pierard O.; Zealouk L.; Goldberg A., *J Mech Phys Solids* **2002**, *50*, 2275.
- [4] Galeski A.; Argon A. S.; Cohen R. E., *Macromolecules* **1988**, *21*, 2761.
- [5] Murthy N. S., *J Polym Sci, Polym Phys* **2006**, *44*, 1763.
- [6] Murthy N. S.; Bray R. G.; Correale S. T., Moore R. A. F., *Polymer* **1995**, *36*, 3863.
- [7] Penel-Pierron, L.; Séguéla, R.; Lefebvre, J.-M., *J Polym Sci, Polym Phys* **2001**, *39*, 484.
- [8] Penel-Pierron L.; Séguéla R.; Lefebvre J.-M.; Miri V.; Depecker C.; Jutigny M.; Pabiot J., *J Polym Sci, Polym Phys* **2001**, *39*, 1224.
- [9] Magill J., *Polymer* **1962**, *3*, 655.
- [10] Magill J., *Polymer* **1965**, *6*, 367.
- [11] Turska E.; Gogolewski S., *Polymer* **1971**, *10*, 616.
- [12] Kyotani M.; Mitsuhashi S., *J Polym Sci, Polym Phys* **1972**, *10*, 1497.
- [13] Hiramani M., *J Macromol Sci, Phys* **1984-85**, *23*, 397.
- [14] Murthy N. S.; Aharoni S. M.; Szollosi A. B., *J Polym Sci, Polym Phys* **1985**, *23*, 2549.
- [15] Landau, L. D.; Lifshitz, E. M., *Elasticity theory*, 1975.
- [16] Ferreiro, V.; Coulon, G., *Journal of Polymer Science: Polymer Physics* **2004**, *42*, 687.